Temporal Structured Classification of Sentinel 1 and 2 Time Series for Crop Type Mapping

Sébastien Giordano, Simon Bailly, Loic Landrieu, Nesrine Chehata

Temporal Structured Classification of Sentinel 1 and 2 Time Series for Crop Type Mapping

Sébastien Giordano[a], Simon Bailly[a], Loic Landrieu[a], Nesrine Chehata[b,a]

[a] *Univ. Paris-Est, LASTIG MATIS, IGN, ENSG, F-94160 Saint-Mande, France*
[b] *EA 4592, G&E Lab, Bordeaux INP/ Bordeaux Montaigne University, France*

Abstract

As part of the EU Common Agricultural Policy (CAP) reform of 2020, each EU member country is expected to suggest new farmland management protocols. Currently, farmers must manually declare each year their crop types into the Land-Parcel Identification Systems (LPIS), a geographic information system identifying the land use of agricultural parcels within each EU member country. Such a protocol remains tedious and error-prone. Automatic Earth observation image analysis can help achieving such a task. Leveraging the recent availability of precise and frequent Sentinel acquisitions, this work aims to automate the LPIS update.

We propose modeling the crop type of parcels from a sequence of (radar and optical) satellite acquisitions, as well as LPIS entries of previous years, with a linear-chain Conditional Random Field. The novelty lies on the fusion of multi-modal images at the feature level and the integration of temporal knowledge extracted from existing land-cover databases. We tested our model on two large-scale French study areas ($\geq 1250\,\mathrm{km}^2$), which are geographically distant and show different agronomic rules: the *Seine et Marne* (North of France) and the *Alpes de Haute-Provence* (South East). We use a granular nomenclature comprised of 25 categories.

Our model demonstrates promising results for the task of automating the LPIS update: 89.0% overall accuracy is reached in *Seine et Marne* (10 categories of the 25 present on the area) and 72.9% in *Alpes de Haute-Provence* (14 categories). We show that the temporal modeling increases the accuracy by +2.6% and +4.6%, respectively.

Keywords: classification, temporal regularization, conditional random fields, agriculture, monitoring, Sentinel images

1. Introduction

1.1. Motivation

The Sentinel 1&2 satellites provide open and free acquisitions exhibiting unprecedented characteristics which are perfectly tailored to agriculture monitoring. Most critically, the high temporal frequency (5-6 days) is very beneficial for identifying crop types. The Sentinel program will be maintained at until at least 2030, which allows us to chronicle both short and long-term evolutions. Besides, the multispectral Sentinel-2 images display relevant spectral bands to agricultural monitoring, that are complementarity to C-Band Sentinel-1 radar images. Finally, the high spatial resolution of both optical and radar images (10-20 m) authorizes parcel-level approaches. For all these reasons, the European Commission strongly recommended the use of the Sentinel programme for reshaping the procedures to monitor the Common Agricultural Policy (CAP) European Commission [1]. This therefore becomes a significant line of research in the forthcoming decade.

In Europe, several use-cases of agricultural monitoring using Sentinel images have been proposed [1], such as crop monitoring (crop area estimates, crop map products, crop phenology indicators), controlling CAP payments with remote sensing (permanent grasslands, greening measures, . . .), updating, and controlling the quality of the Land Parcel Identification System (LPIS) or precision farming at the farm-level.

In this paper, we focus on *automating crop type mapping*. In Europe, the agricultural land cover information is manually updated yearly by the farmers themselves. They input the type and surface area of their parcels. This manual declaration is complicated for farmers, error-prone and leads to expensive control procedures by external agencies. In this context, a pre-filled agricultural declaration based on supervised classification techniques would allow the farmers to only have to validate the declaration, cutting down on control and input errors. The automation of crop type declarations requires a robust classification model, based on Sentinel images observations but also on ancillary data such as LPIS archives to improve the classification results.

Indeed, the crop type identification may be improved using *a priori* knowledge on management practices and especially on crop rotations per parcel. The choice of the crop type and agricultural practices on a parcel are strongly dependent on past events over previous years. The LPIS archives provide such information. Modeling these temporal structures in combination with the Sentinel image time series can lead to significant gains in classification accuracy. In this paper, we focus on benefiting from *crop rotation knowledge*.

1.2. Related work

1.2.1. Multi-temporal satellite images for crop mapping

In the literature, many studies showed the potential of multi-temporal satellite images for crop type mapping [2]. Inglada et al. [3] assessed state-of-the-art methods for automatic crop mapping with multi-temporal and very high spatial resolution optical images. For this purpose, five different classification approaches using SPOT4 and Landsat-8 images were compared on 12 different study areas worldwide. Best results (Overall accuracy of 80% for 6 annual crop classes) were obtained with the Random Forest classifier [4]. Immitzer et al. [5] used mono-temporal Sentinel-2 images for agricultural and forest land cover classification. A multi-temporal approach has been proposed by Kussul et al. [6]. Landsat-8 and Sentinel-1 time series were used on a study area in Ukraine. A pixel-based classification accompanied with a parcel-based regularization (majority voting) was proposed using LPIS ancillary data. An overall accuracy of 89% was reached but the nomenclature was limited to 6 annual crops (Winter wheat, Winter rapeseed, Maize, Sugar beet, Sunflower, Soybeans) and large parcels were generally considered ($> 250\,\text{ha}$). More recently, experiments were led at the country level (Czech Republic) by the Sen2-Agri consortium [7]. A multi-sensor (Sentinel-1, Sentinel-2) pixel-based supervised classification was performed. The LPIS was used for both learning and validation steps. A crop map was produced every month using Sentinel-1 radar images (December to September) and Sentinel-2 optical images (March to September). The overall accuracy was greater than 80% and each land cover type had a F-score greater than 60%. The quality of the classification was further increased as more data was acquired. However, the nomenclature was here again very limited (7 classes) and does not fully integrate temporal knowledge from existing data.

Two major aspects of the state-of-art of crop type classification remain to be improved in order to obtain a reliable pre-filled declaration system: the precision on small parcels and the granularity of the nomenclature.

1.2.2. Crop rotation consideration

Crop rotations are known to be useful management practices, improving agricultural yields [8] and soil quality [9]. References in literature on their role in agriculture are numerous [10]. To take into account crop rotations in crop type prediction, two questions have to be answered: (i) how to model the crop rotations? (ii) how to integrate crop rotations in a land cover classification process?

1.2.3. Modeling crop rotations

Two different approaches can be used to model rotations. The first one consists in using *a priori* agronomist expert knowledge. The second one would be to automatically learn crop rotations from the statistical analysis of past practices, as found in the LPIS archives. The crop rotation knowledge can then be modeled with a common representation in agronomy: transition matrices representing transition probabilities between crop types from year to year.

The ROTAT model [11] is based on expert knowledge. The tool automatically generates all possible crop rotations over an area and performs a selection taking expert knowledge into account. Castellazzi et al. [12] introduce a mathematical framework based on transition matrices to model crop rotations at the landscape scale. Dury et al. [13] review various crop rotation models and emphasize that these models are too static. To improve the models, the authors propose integrating different time scale dynamics. Indeed, crop rotation models have several limitations. The information is never available at the parcel scale. The models are strongly dependent on the study area; they cannot adapt to environmental or agricultural management changes. Some studies have been proposed to overcome these limitations. Aurbacher and Dabbert [14] underline the importance of having rotation information at the parcel-level and consequently propose to use Markov chains. Concerning adaptation capacities to different study areas, Detlefsen and Jensen [15] use network modeling techniques to find on a given parcel the optimal rotations knowing a selection of crops. Finally, the influence of environmental changes such as global warming on agricultural practices has been studied by Olesen et al. [16], then modeled by Aurbacher et al. [17]. Nevertheless, few studies take this parameter into account in crop rotation models.

Learning rotations using past data on crop types is a way of overcoming the limitations of *a priori* expert knowledge approaches.Both approches can also be successfully combined. For instance, the CarrotAge tool [18] allows to perform a spatio-temporal analysis by training a Hidden Markov Models with a land cover database. Results are thereafter interpreted by an agronomist in order to be integrated in soil or water management studies. Another example is the CropRota method [19] that combines agronomic criteria and land cover information to generate crop models at the farm or region levels. The ROTOR model [20] relies on control sampled farms, field surveys and expert knowledge. These three models can take into account changes in agricultural practices or study areas. However, expert knowledge is still required, and such models can not be used at the parcel level.

The parcel-level crop information provides a finer crop type nomenclature but needs heavy field surveys and more complex models than those described above. Xiao et al. [21] used such parcel-based information to describe the spatial distribution of crop sequences at a large regional scale, but with a limited 3-class nomenclature. For many years, several European countries as well as the United States maintain and annually update a geographical information system on agricultural parcels, i.e. the Land Parcel Identification System (LPIS) [22]. Parcel-based crop rotation information at a national scale can be derived by exploiting past annual versions of the LPIS. The information on environmental or agricultural changes is then implicitly contained in these data. Several studies proposed to use the LPIS to study and model crop rotations. Leteinturier et al. [23] used several years of LPIS to compute crop rotation indicators. More recently, Osman et al. [24] produced and assessed a land cover classification based on the former version of the French LPIS.

1.2.4. Integrating crop rotations into classification pipelines

Only few studies have focused on the integration of crop rotation information into classification pipelines. Osman et al. [24] studied early crop mapping using only the LPIS. A prediction model based on Markov logic was proposed, but not in combination with remote sensing observations. Results showed that this model has better classification precision than models based on remote sensing observations at the beginning of the crop growing season. This is mainly due to the fact that few satellite images are available at the beginning of growing season and that crops are hard to distinguish at this development stage: observation-based classification is unreliable compared to temporal prediction. This statement remains to be confirmed with the use of higher temporal resolution Sentinel images. Other studies proposed to introduce a temporal structure, using the Hidden Markov Chains, in a classification pipeline but they aim at modeling phenology instead of crop rotations [25, 26, 27]. Modeling phenology is useful to detect optimal temporal intervals to acquire remote sensing images for crop mapping [28]. Kenduiywoa et al. [29] modeled phenology information into a Conditional Random Field, but the classification is performed at different dates through the year.

1.3. Specific objectives

The general objective of this article is to assess the feasibility of a pre-filled agricultural declaration based on Sentinel 1+2 images for crop types and surfaces. This paper focuses on crop type predictions. Related work described in Section 1.2, allow us to formulate the following specific objectives:

- **Thematic contribution**. Sentinel images are part of a recent satellite program (October 2014 and December 2015 for radar and optical images, respectively). Few research studies have yet assessed the crop type prediction accuracies that could be obtained with these time series. This study will especially focus on using an exhaustive national crop nomenclature, the consideration of all agricultural parcels (with no minimal crop area consideration), and the complementarity between Sentinel-1 and Sentinel-2 images.

- **Methodological contribution**. Crop rotations have rarely been combined with satellite observations into a classification pipeline. Our objective is to propose a method that integrates the crop rotation temporal structure into the classification process and to assess the capacity of the proposed method to improve crop type prediction accuracies.

Sentinel data, LPIS, and the study sites will be described in Section 2 as well as the necessary image and vector preprocessing steps. Two study sites with very different agricultural management practices and parcel sizes are chosen. In Section 3, we propose a parcel-based classification with a Random Forest classifier [4] and a temporal-structured framework to integrate crop rotation information. Results are given and discussed in Section 4. The models learned for the LPIS crop rotations and land cover prediction from the Sentinel images are first assessed independently. A combination of both models is finally evaluated and discussed.

2. Site and material

2.1. Study sites

In order to assess the feasibility of a pre-filled declaration of crop types, two complementary large-scale sites were chosen in France. The characteristics and location of each site are provided in Figure 1 and Table 1.

The first one is located in South Eastern France, in the Alpes de Haute-Provence region, in the Durance river Valley. It is representative of a Mediterranean cultivated area. This site will be called *Site04* in reference to the national number of the corresponding region. It covers 1050 km^2 and is characterized by a highly variable topography, a very fragmented parcellar while giving a high diversity of crop types. The site is an observatory of the French mapping agency (IGN) where crop observations are made annually.

The second one is located near Paris, in the Seine et Marne region, at the north of Coulommiers town. It covers 233 km^2. Contrarily to the *Site04*, this site is characterized by a flat relief, with a large parcellar and a majority of cereal crops. This site is a permanent observatory of a Group of Scientific Interest; GIS Oracle (http://gisoracle.irstea.fr/). This site will be noted *Site77* in reference to the national number of the corresponding region.

Table 1 illustrates the difference of both sites in terms of covered area and cultivated crop types. Figure 3 gives for both sites the normalized histograms of parcels area. Figures 4 and 5, show *Site04* and *Site77*, respectively, with the corresponding parcels and nomenclatures.

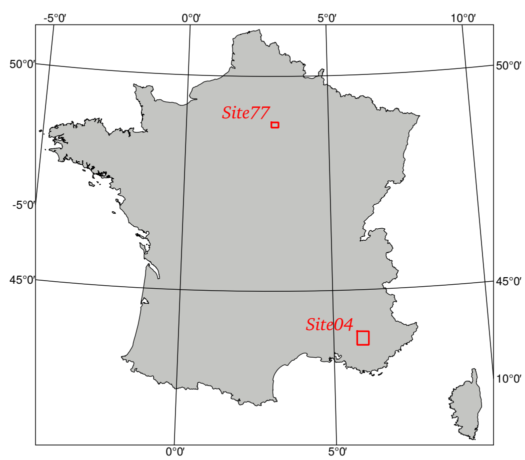

Figure 1: Localisation of *Site04* and *Site77*

2.2. Land Parcellar Identification system

In France, the Land Parcellar Identification System is called *Registre Parcellaire Graphique* (RPG). It is available on the whole territory since 2002. It corresponds to a Geographic Information System (GIS) of cultivated and non cultivated areas (NCA) that may correspond to isolated trees, hedges, groves, artificial areas . . . For cultivated areas, the RPG gathers the geometric information (i.e., the parcel delimitation) and the corresponding semantic information allowing to identify each agricultural parcel such as the owner, the operator, the area, the crop type etc (*cf.* Figure 2).

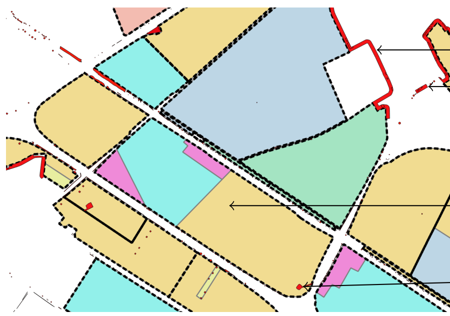

Figure 2: Details of the French LPIS (RPG). (a) Non cultivated areas (NCA); (b) a block of contiguous parcels, belonging to the same operator (dashed lines); (c) a Parcel, defined by its owner, operator, surface, crop type. . .

All this information has to be entered in April-May period for each year by the farmers. Until 2014, the declarations were made at a parcel block scale for contiguous parcels with the same operator. Since 2015, the declarations are made at the parcel scale. The crop type is specified among more than 300 sub-classes, which are organized into 28 classes. This study focuses on a parcel-based approach. Thus, to be in tune with Sentinel-2 images availability, only the 2016 parcel-based RPG edition is used for training and validation. The geometrically stable blocks of parcels from 2010 to 2014 (available LPIS data) were used to learn crop rotations. The latter step was processed on the corresponding departments of both sites ((77): $5915\,\mathrm{km}^2$ and (04): $6925\,\mathrm{km}^2$), in order to get more robust crop type transitions.

2.3. Nomenclature

The 28-class nomenclature used in the RPG declarations is driven agricultural monitoring needs: hence, it exhibits a fine-grained categorization. However, some classes are indistinguishable from purely remote sensing observations, such as lands left in fallow for different amount of times. Consequently, we present in Table 1 a slightly adjusted nomenclature of 25 classes. 14 and 10 of these classes are present on *Site04* and *Site77*, respectively.

Class	**# parcels - *Site04***	**# parcels - *Site77***
Corn	147	350
Barley	517	158
Other cereals	2176	889
Rape seed	154	85
Sun flower	293	✗
Other oilseeds	116	✗
Protein(peas)	87	76
Fiber plants	✗	76
Forage crops	1215	46
Meadows	3652	725
Fruit trees	298	30
Vignards	249	✗
Olive groves	1029	✗
Aromatic crops	1452	✗
Vegetables	520	131
Total nb classes	14	10
Total nb parcels	11905	2566
Site area (km^2)	1050	233
Total nb stable parcels 2015/2016	9230	1902
Total transitions 2010-14	29478	36891

Table 1: Comparison of both study sites in terms of area and crop types.

Figure 3 shows the distribution of parcel sizes on both sites. One can see that *Site04* is much more fragmented with very small parcels while *Site 77* shows large parcels reaching 20 ha.

Figures 4 and 5 show the 2016 RPG edition i.e., the ground truth data on *Site04* and *Site77* respectively, with the corresponding classes on each site. One can observe that, on *Site04*, dominant crops are: *cereals* (23.8%), *meadows* (30.7%), *aromatic crops* (12.2%), *forage crops* (10.2%) and *olive groves* (8.6%). For *Site77*, two dominant crops are present: *cereals* (57.7%), *meadows* (28.3%), followed by *vegetables* (5.1%). The data are much more imbalanced in the latter case, making the *77* classification task more complex.

2.4. Multimodal Sentinel-1 & Sentinel-2 images

Our framework is fed with multimodal and temporal Sentinel images dedicated to agricultural applications and environmental monitoring. The

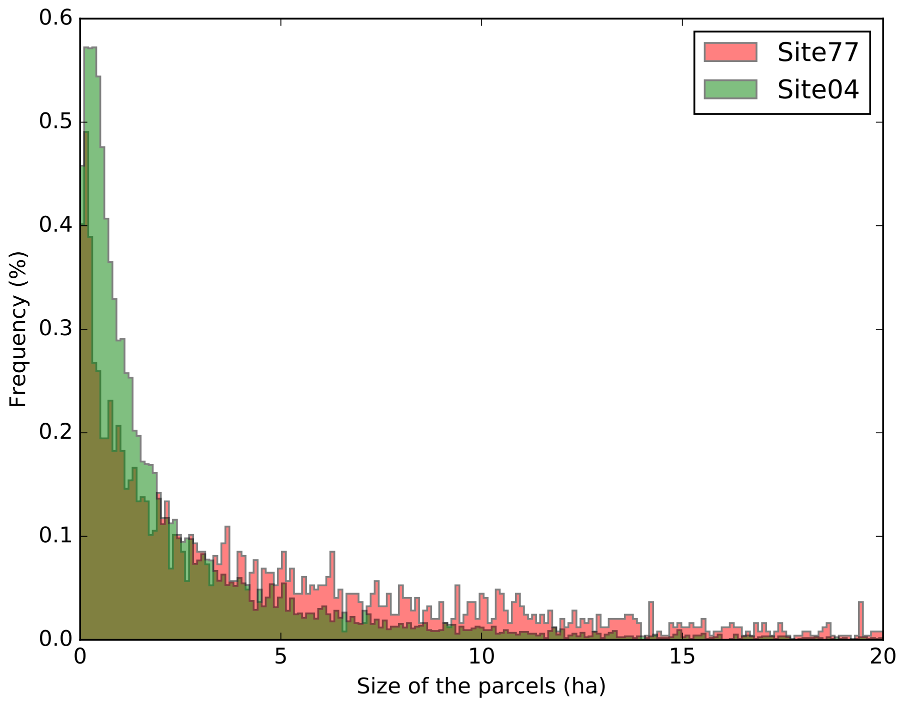

Figure 3: Normalized histogram of parcel area for *Site04* and *Site77*.

high spectral resolution of the images and high temporal sampling rate make these acquisitions particularly well-suited for crop mapping (Table 2). Sentinel-1 (S1) sensor provides band-C SAR images while Sentinel-2 (S2) provides multispectral images.

Figure 6 shows a Sentinel-2 optical and a Sentinel-1 radar acquisitions on *Site04*, more precisely on *Oraison* Village.

Sentinel-2 (S2) is a multispectral sensor with 13 bands covering the VIS-SWIR domain, which measures the reflectance of surface objects in different optical domains. In particular, its near infra-red (NIR) and red-edge bands allow a fine characterization of crops. Sentinel-1 is a C-band SAR. This allows to measure scattering coefficients that are related to an emitted waveform ($\lambda = 5.5\,\text{cm}$ in C-band). The recorded energy depends on the characteristics of the encountered object (slope, roughness, humidity,etc.) and on the emitted waveform (wavelength, polarization). Sentinel-1 has different acquisition

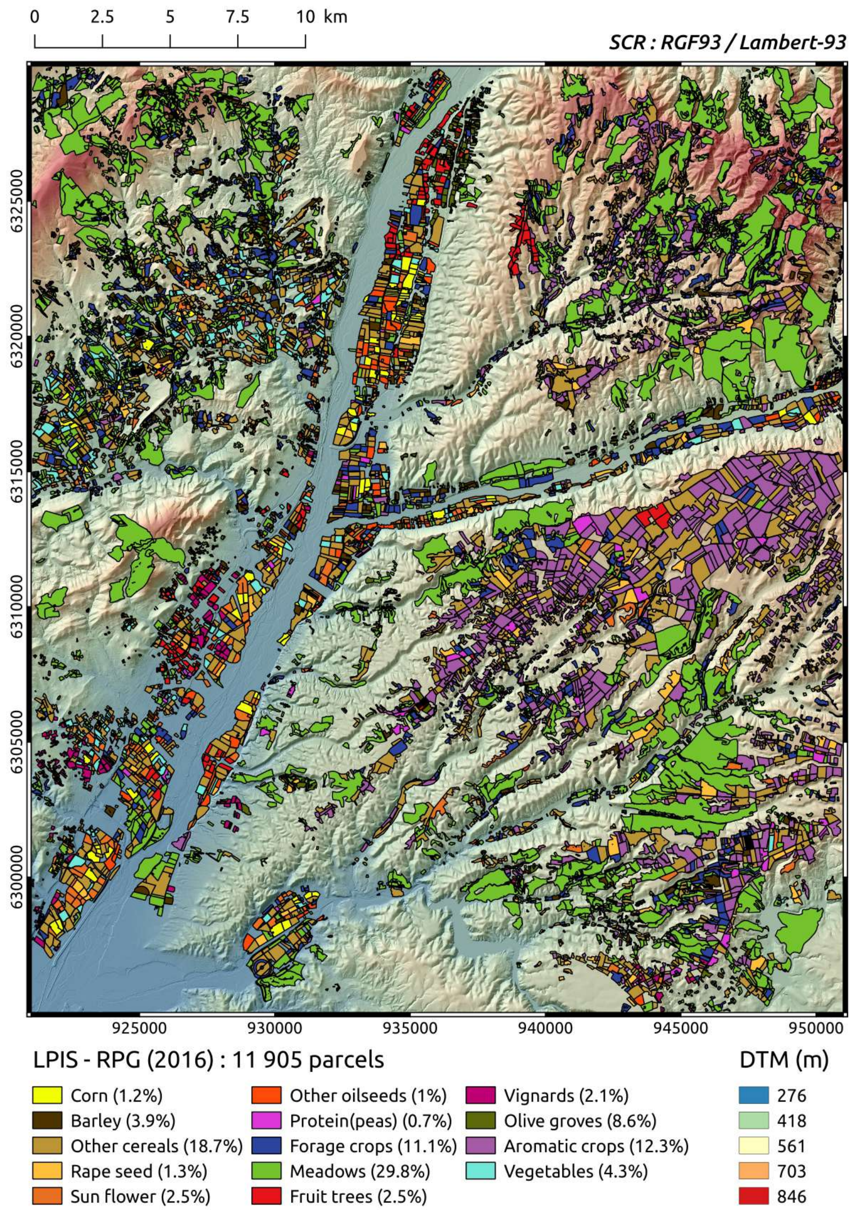

Figure 4: *Site04*: 2016 RPG parcellar superimposed to a very high resolution Digital Terrain Model.

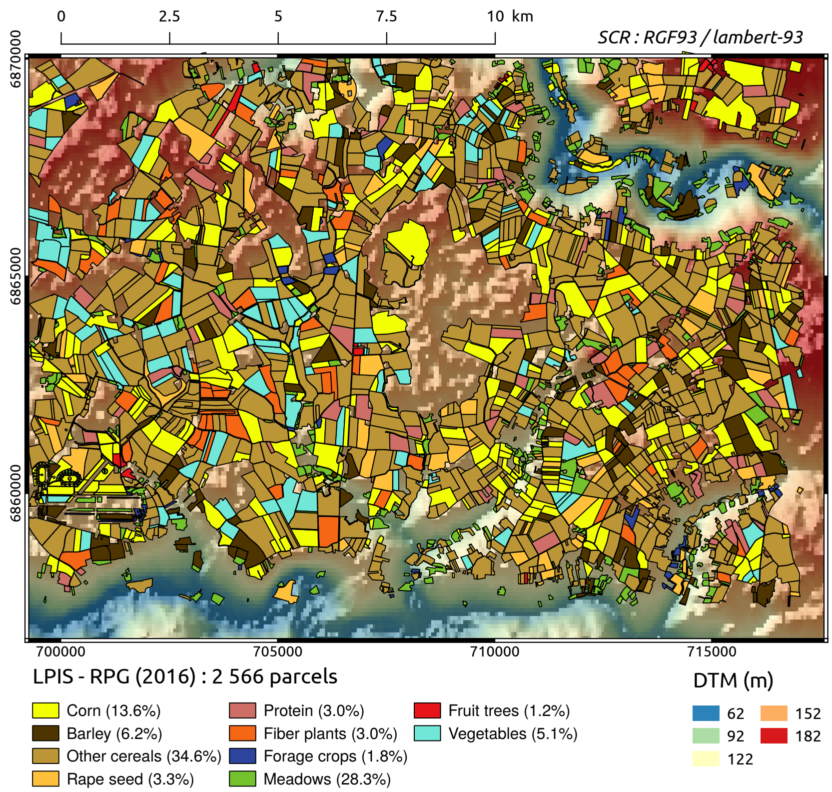

Figure 5: *Site77*: 2016 RPG parcellar superimposed to a SRTM Digital Terrain Model.

	Acquisition date	Sensor	Characteristics
Sentinel-1	3 April 2014 (S1A) 25 April 2016 (S1B)	C-SAR (5,4 GHz)	Cycle: 12 jours # satellites: 2 (S1A et S1B) Revisit period: 6 days Resolution: 5·20 m by default (mode IW) Polarization: dual (VV,VH)
Sentinel-2	23 June 2015 (S2-A) 7 March 2017 (S2-B)	Multispectral image	Cycle: 10 days # satellites: 2 (S2A et S2B) Revisit period: 5 days Resolution: 10 m - 60 m according to band Spectral: 13 bands (2 NIR and 3 Red-edge)

Table 2: Characteristics of Sentinel sensors and used images: Sentinel-1, Sentinel-2.

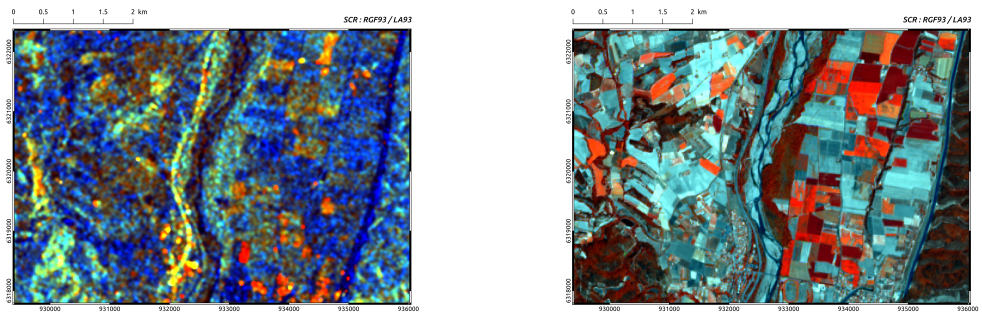

Figure 6: *Site04*, focus on Oraison village: Sentinel-1 (5 Aug. 2015). Composed color image with different polarizations related to retrodiffusion coefficients: σ_{vv}, σ_{vh}, $\frac{\sigma_{vh}}{\sigma_{vv}}$. Site04-Oraison village: Color-infrared Sentinel-2 (3 Aug. 2015). See text for more details.

modes that differ according to observed surface, sensor spatial resolution and polarization. The available mode on the studied sites was the Interferometric Wide (IW) mode. This mode presents a dual polarization:

- VV : Incident waveform is polarized vertically and the antenna records it vertically. This polarization allows us to characterize the soil roughness.

- VH : Incident waveform is polarized vertically and the antenna records it horizontally. This polarization provides volumetric information on vegetation.

In addition, we use directly the GRD (*Ground Range Detected*) image format, which corresponds to the average of approximately five Single Look Complex ((SLC) acquisitions corrected by the incidence angle and resampled at 10 m spatial resolution (Section 2.5.2).

2.5. Sentinel image pre-processing

Figure 7 illustrates the optical and radar pre-processing steps to obtain parcel-based features that will be fed into our classification workflow.

2.5.1. Sentinel images repositories

Sentinel images are available on several platforms: the *Copernicus scihub* (https://scihub.copernicus.eu/) at the European level, the scihub mirror *Peps* (https://peps.cnes.fr) and the downstream service *Theia* (https://www.theia-land.fr/) at the French national level. Sentinel-2 images (10 bands) were automatically downloaded from the *Theia* platform as they were

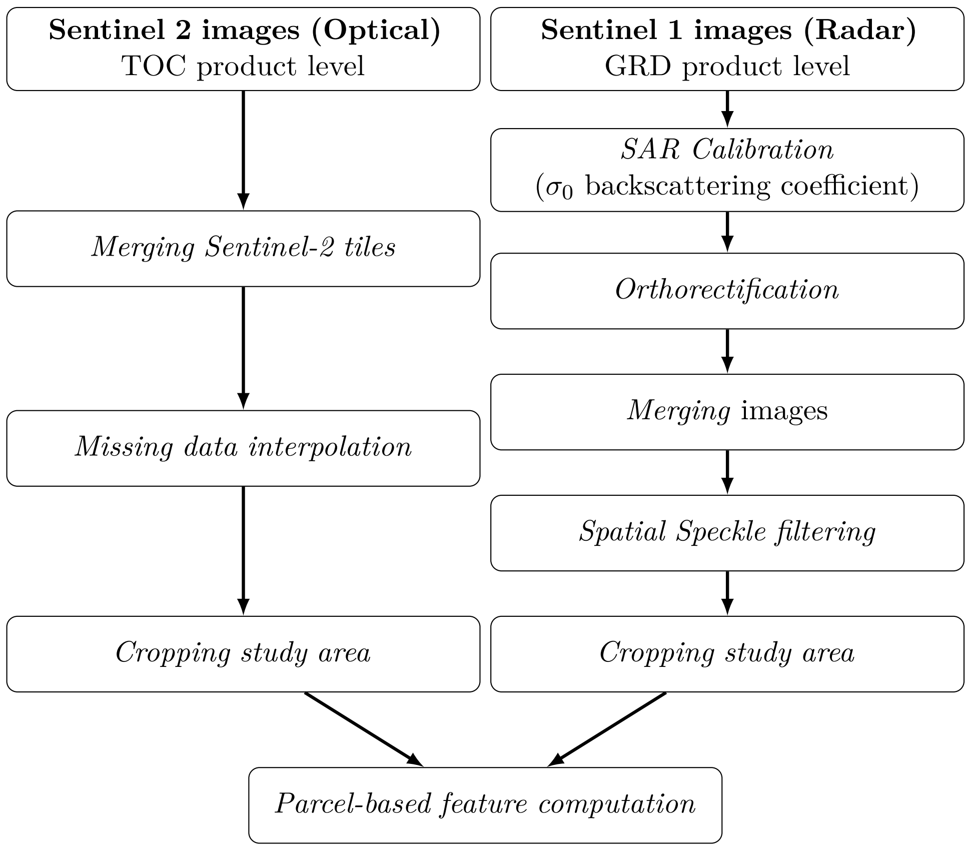

Figure 7: Sentinel-1 and 2 pre-processing steps

available in tiled format, calibrated as Top of Canopy (TOC) reflectance and accompanied with robust cloud mask information. Radar Sentinel-1 images were downloaded from the *Peps* platform in the Ground Range Detected format (GRD). The total number of images is illustrated in Table 3 and confirms the complementarity between Sentinel-1 and Sentinel-2 images, where the latter may suffer from an important cloud cover while Sentinel-1 radar images allow to get more information. For instance, on *Site77*, particularly obstructed by cloudy skies, Sentinel-2 images (12) are 7 times fewer than the S1 images (85). On the particular Sentinel-2 orbit covering the *Site77* study area, many acquisition problems occurred in 2016. On the contrary, *Site77* is located where ascendant Sentinel-1 images overlap making the available radar images more numerous.

2.5.2. *Sentinel 1 pre-process*

The dual polarization GRD S1 images were first calibrated to σ_0 radar backscattering coefficient. Then, the orthorectification was performed using the SRTM digital terrain model and the georeferencing information supplied with the GRD files. The speckle is partly removed using a simple 5×5 Lee filter [30]. The information was then averaged at the parcel level. In addition to VV and VH radar features, an extra radar feature ($\frac{\sigma_{0_{VH}}}{\sigma_{0_{VV}}}$) was derived. This ratio is known to be more robust to acquisition system errors or environmental factors such as soil moisture. As a result, Veloso et al. [31] argue that it is a more temporal stable indicator than the $\sigma_{0_{VV}}$ et $\sigma_{0_{VH}}$ backscattering coefficient.

Average and standard deviation of these three features per radar image are then computed for each date and for each parcel of the study sites. The number of obtained features are shown in Table 3 .

Site	Nb of dates	Optical features	Radar features	Total
04	Optical: 23 Radar: 28	20 per image (σ and μ of 10 bands + NDVI)	6 per image (σ and μ of 3 radar features)	Optical: 460 Radar: 168 **total: 628**
77	Optical: 12 Radar: 85	20 per image (σ and μ of 10 bands)	6 per image (σ and μ of 3 radar features)	Optical: 240 Radar: 509 **total: 749**

Table 3: Characteristics of the parcel-based features for both sites. See text for more details.

2.5.3. *Sentinel 2 pre-process*

Sentinel-2 images downloaded from *Theia* platform were already orthorectified in a cartographic system and calibrated in TOC reflectance. When the study area covered more than one tile, the corresponding tiles and cloud masks were merged. On *Site77*, only 12 Sentinel-2 optical images were obtained in 2016 as shown in Figure 8 with corresponding cloud cover whereas 23 images are available on *Site04*. The missing data (clouds) were filled using a multi-temporal spline interpolation [32]. Average and standard deviation of the 10 spectral bands per optical image were then computed for each date and for each parcel of the study sites. The number of obtained features are shown in Table 3.

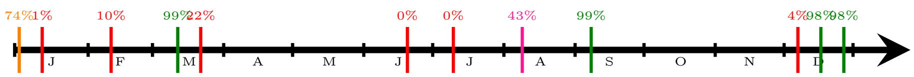

Figure 8: S2 optical images over the year 2016 and corresponding cloud cover on *Site77*.

2.6. LPIS pre-process

Seven editions of the French LPIS were used. From 2010 to 2014, the crop type is defined at the block level (Figure 2) (i.e., the majority crop type of the block) with a nomenclature of 28 classes. For 2015 and 2016 editions, the crop type is known at the parcel-level with a detailed nomenclature (over 300 classes). In order to use all available editions, all LPIS were aggregated to the 25 considered classes. Geometrically stable parcels were identified using a GIS spatial join between 2015 and 2016 versions. The number of stable parcels for both sites is given in Table 1. The 2016 stable parcels were used for training and validation of the supervised classification model (Section 3.1). The 2015 stable parcels were necessary to train the temporal structured method (Section 3.2). Finally, a similar GIS spatial join was performed at the block level for 2010-2014 LPIS editions, over the whole corresponding regions (04 and 77) in order to get more robust crop transitions. Thus, a 5-year series of crop type transitions were obtained on stable blocks over both 04 and 77 regions. The number of transitions for each study site is given in Table 1. These transitions will be used in the temporal structure estimation (Section 3.2.1).

3. Methodology

Our method can be broken down into two components: parcel-wise classification and temporal modeling. The first part aims to predict the crop types per parcel using Sentinel time series with no temporal structure. The second component consists in integrating into a structured model the temporal structure derived from previous LPIS editions and based on crop rotations.

3.1. Parcel-based multi-source classification

The first step in our pipeline is crafting discriminative features from sequential satellite acquisitions. For each parcel, we consider all available (and interpolated) optical and radar data over one year. To obtain parcel-based rather than pixel-based features, we consider the average and standard deviation of each spectral band over the pixels composing the parcel. Those attributes are aggregated into a tensor of dimensions equal to twice the number of acquisitions over the year for each parcel.

We then perform feature selection by iteratively removing the features with the least *importance* until the cross-validated classification score starts decreasing over our learning set. For a given parcel i and a given year t we denote $X_i^{(t)} \in \mathbb{R}^D$ the tensor of aggregated selected features, with D the selected feature size. As certain classes were over-represented in our data sets, each class is weighted proportionally to the square root of the inverse of its number of instances.

A Random Forest classifier is selected for the classification task. It provides parcel-wise prediction under the form of a pseudo-probability.

3.2. Temporal-structured classification of parcels

We now consider the temporal structure of each parcel independently. We denote by $X_i \in \mathbb{R}^{T \times D}$ the sequence of features $X_i^{(t)} \in \mathbb{R}^d$ for the parcel i for the years $t = 1, \cdots, T$. Likewise, we denote $Y \in \mathcal{K}^{N \times T}$ the labels of each parcel for each observed year with $\mathcal{K}$ the set of all possible labels.

3.2.1. Temporal structure

The aim of this step is to model the yearly crop rotations in order to improve crop type prediction.

As stated in 1.2.2, crop rotation has a significant impact on land cover. This dependency is modeled with a discriminative linear chain Conditional Random Field (CRF) of order m, as shown in Figure 9. For a parcel i, we model the posterior distribution $P(Y_i \mid X_i)$ of the labels Y_i given the observed features X_i as:

$$P(Y_i \mid X_i) = \frac{1}{Z} \exp\left(\sum_{t=1}^{T} O(Y_i^{(t)}, X_i) + \sum_{t=m+1}^{T} I(Y_i^{(t-m)}, \cdots, Y_i^{(t)}, X)\right), \quad (1)$$

where Z is a normalizing factor, O the observation potential, and I the interaction potential, described below.

Observation potential: The observation potential models the link between the observed features and the label of each parcel. $O(Y_i^{(t)}, X_i)$ is taken as the logarithm of the pseudo-probability given by the random forest classifier, described in Section 3.1.

Interaction potential: This potential models the temporal dependencies between the parcel's labels. We model this potential as the transition probability from a sequence $Y_i^{(t-m)}, \cdots, Y_i^{(t-1)}$ to a label $Y_i^{(t)}$. For the sake of simplicity, we choose an homogeneous parameterization, independent of the observed features, and shared by all parcels and years:

$$I(Y_i^{(t-m)}, \cdots, Y_i^{(t)}, X) = \log\left(M(Y_i^{(t-m)}, \cdots, Y_i^{(t)})\right),$$

with $M \in \mathbb{R}_+^{k^m}$ a tensor such that $\sum_{\{i_1,\cdots,i_{m-1}\}\in\mathcal{K}^{m-1}} M_{i_1,\cdots,i_{m-1},i_m} = 1$ for all $i_m \in \mathcal{K}$. This tensor can be interpreted as a transition probability from a sequence in $\mathcal{K}^{m-1}$ to a label in $\mathcal{K}$ [33].

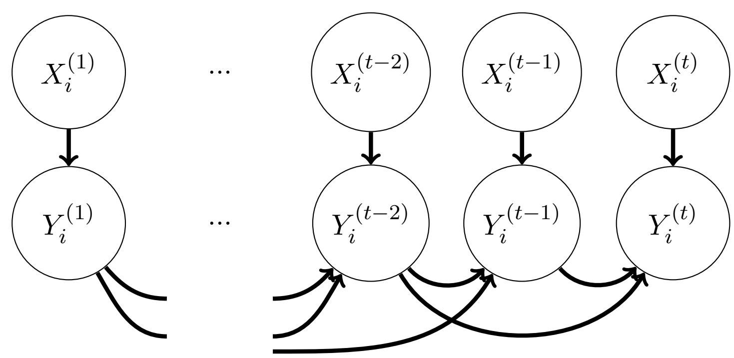

Figure 9: Graph structure of the temporal dependency at order 2.

3.3. Learning

The observation potential is obtained by training the random forest classifier. Learning the transition tensor $\hat{M}$ from labeled data can be done in close form. For $i_1, \ldots, i_m \in \mathcal{K}^m$, let:

$$\hat{M}_{i_1,\ldots,i_m} = \frac{N_{i_1,\ldots,i_m}}{N_{i_1,\ldots,i_{m-1}}},$$

with $N_{i_1,\ldots,i_m}$ the number of sequences $i_1, \ldots, i_m$ observed in the labeled data for all parcels and all years, and $N_{i_1,\ldots,i_{m-1}}$ the number of sequences $i_1, \ldots, i_{m-1}$ observed for the $T - m$ first years.

To account for the large size of this matrix (k^m) and to prevent numeric issues, we perform a Laplacian smoothing with $\alpha = 1$ as described in Manning et al. [34, 11.3.2].

3.4. Inference

The aim of this step is to predict the label $Y_i^{(t)}$ from the labels and observations of the previous years for an unseen parcel. This can be directly computed by injecting the observation and interaction potentials obtained from the trained models into

$$p(Y_i^{(t)} = k \mid Y_i^{(t-m,\cdots,t-1)}, X_i) \propto \exp\left(O(k, X_i^{(t)}) + I(Y_i^{(t-m)}, \cdots, Y_i^{(t-1)}, k)\right),$$

and normalizing the results to obtain a probability.

4. Results and discussions

In this section, we present the experimental setup and the evaluation metrics. Results are illustrated on both sites and will be discussed with regard to methodological and thematic objectives presented in Section 1.3.

4.1. Experimental setup

The random forest classifier is composed of 100 decision trees. The meta-parameters of the forest, such as the maximum number of attributes considered at each node, are chosen by k-fold cross-validation with $k = 4$.

For the temporal structure, spatio-temporal homogeneity hypothesis allows us to estimate the transition tensor $\hat{M}$. For each study site, only the geometrically-stable parcel-blocks over the corresponding departments and a period of 5 years are used. The number of 5-year transitions that contribute to estimate $\hat{M}$ is given in Table 1.

The data is randomly split equally into a training and a testing sets. In practice, the availability of numerous LPIS editions allows us to have a high number of training parcels. The model is trained and validated on the training set while the quality of the model is estimated on the testing set. The overall accuracy (OA) is used to assess the general performance of the model, while the F-score for each class allows us to estimate the per-class quality. To sum up this information, the F-scores are averaged, with and without weighting by the class cardinality. The results are given as an average over 10 runs of the random forest classifier.

4.2. Transition matrix assessment

The transitions were computed on geometrically stable parcels between 2010-2014. In this study, only first order transitions were computed, i.e.,

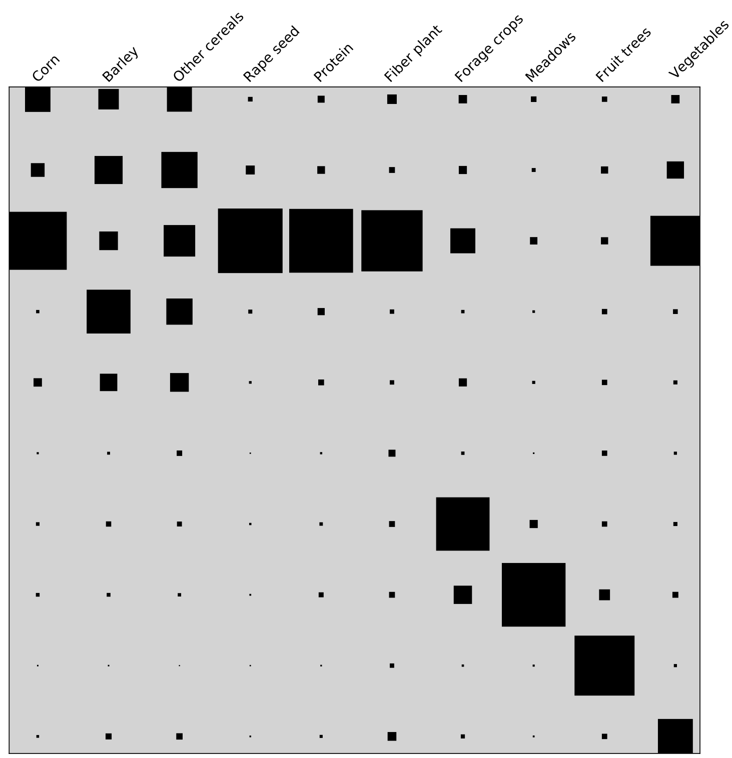

Figure 10: *Site 77* - Representation of the transition matrix with a Hinton diagram.

between one given year and the previous year. Figures 10 and 11 give the estimated transitions between crop classes as Hinton diagrams, for both sites.

On *Site04*, the most probable transitions are to and from permanent crops, such as *olive groves*, *vignards*, *orchards*, *estive landes*, *meadows* and *fruit trees* reaching 98.34%, 93.87%, 92.72%, 98.31%, 91.89% and 84.23%, respectively. From the transition matrix, we can observe that the standard rotation patterns of annual crops are generally not applied in this area. The *rape seed*, *proteins* and *sun flowers* have probabilities of 76.53%, 66.78% and 64.25%, respectively to be transformed to *other cereals* the following year.

On *Site77*, the most probable transitions are conversely observed for the annual crops. Agronomical rules for annual crops rotation seems to be much more enforced in this area. The *rape seed* and *proteins* have probabilities of 97.09% and 94.85%, respectively to be transformed to *other cereals* the following year. The *rapeseed* → *winter wheat* (in *other cereals*) → *barley* is a

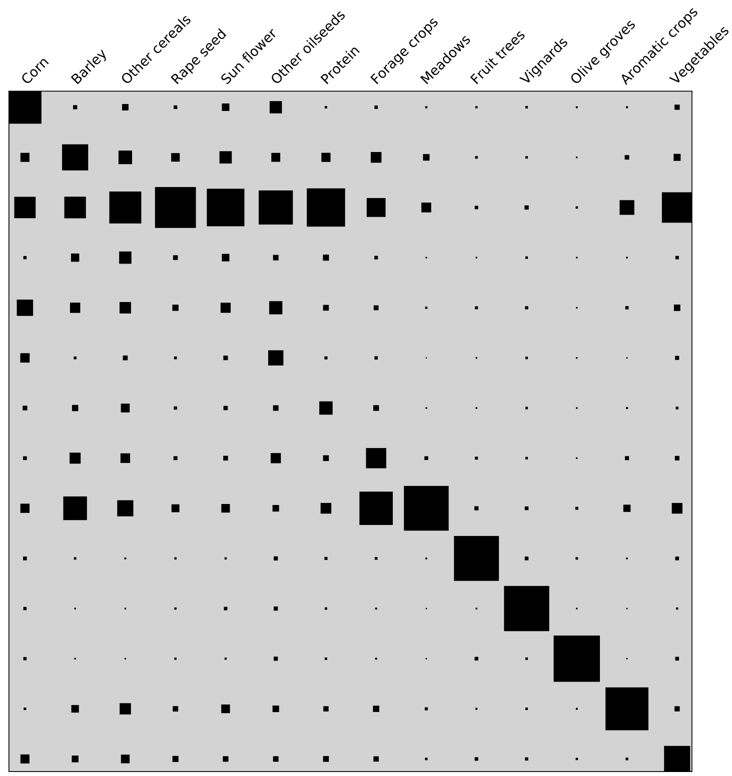

Figure 11: *Site 04* - Representation of the transition matrix with a Hinton diagram.

well-known 3-year rotation for farmers of this area. Permanent crops such as *meadows*, *orchards*, *fruit trees*, *vineyards* have a probability of being carried over the next year of 94.45%, 83.65%, 81.39% and 62.12%, respectively.

4.3. Quantitative and qualitative analysis

This section illustrates prediction accuracies using different feature combinations and both unstructured and structured approaches.

4.3.1. Quantitative evaluation on Site04

From the results displayed in Table 4, one can see that for parcel-based crop type prediction using image observations, optical data give better results than radar data (+9.1% for OA and +10.4% for weighted F-score). This can be explained by the finer resolution of optical imagery, as well as the small parcel size of *Site04* (*cf.* Section 4.3.2. Furthermore, *Site04* being situated in sunny Southern France, it has generally little cloud cover, making optical data very available.

Table 4: Global prediction accuracies on *Site04*, using different feature and methodological configurations.

Unstructured			
Config	OA	F-score	Weighted F-score
Radar	0.639	0.587	0.610
Optical	0.730	0.669	0.714
Radar Optical	0.729	0.679	0.713
Structured			
Radar	0.757	0.592	0.698
Optical	0.776	0.627	0.725
Radar Optical	0.775	0.645	0.723

The results confirm that optical and radar combination leads to the best results in both unstructured and structured approaches.However, the global results remain low for this site, with F-scores varying between 0.58 and 0.64. This is due to the very small size of parcels and highly imbalanced classes. For example, parcels of permanent classes (*meadows*, *fruit trees*, *vignards*, *olive groves*) are overrepresented, as shown in Figure 4.

The confusion matrix for unstructured optical/radar configuration (Table 6) shows that most ambiguities occur on *meadows* classes, *other cereals* and *forage crops*. When integrating the temporal structure, the overall accuracy is improved by 4.6%. Moreover, while the OA using radar data is very low (63.9%), it is improved by the structured approach by 11.8%, confirming the impact of temporal structure even if the accuracy of the parcel-wise prediction is low.

In Table 5, we display the F-score, recall, and accuracy measures per class for both unstructured and structured approaches using radar and optical combination.

As for per-class accuracies, temporal structure highly improves the accuracies of permanent crops (fruit trees +36%, vignards +29.7%, olive groves +25.6%, aromatic groves +19%) reaching F-scores higher than 92.9%. The F-score for *meadows* (permanent and temporary) is improved by 4.1%. These

Table 5: Effect of temporal structure on Classification metrics on *Site04*, using aggregated radar and optical attributes.

	Unstructured			**Structured**		
Class	F score	Recall	Precision	F score	Recall	Precision
Corn	0.888	0.953	0.832	0.780	0.836	0.732
Barley	0.393	0.848	0.256	0.185	0.673	0.107
Other cereals	0.846	0.830	0.862	0.783	0.730	0.845
Rape seed	0.923	1	0.857	0.712	1	0.554
Sun flower	0.789	0.785	0.793	0.713	0.749	0.681
Other oilseeds	0.570	0.745	0.463	0.408	1	0.258
Protein	0.484	1	0.321	0	0.0714	0
Forage crops	0.469	0.735	0.344	0.096	0.884	0.051
Meadows	0.759	0.675	0.867	0.800	0.674	0.983
Fruit trees	0.609	0.863	0.471	0.969	0.962	0.975
Vignards	0.690	0.740	0.646	0.987	0.996	0.979
Olive groves	0.737	0.819	0.670	0.993	0.997	0.989
Aromatic crops	0.739	0.646	0.864	0.929	0.938	0.921
Vegetables	0.611	0.725	0.529	0.674	0.891	0.542

results were expected since the permanent crops have the highest transition probability as shown in Section 4.2.

However, F-scores of annual crops classes decrease when using temporal structure; only slightly so for corn, other cereal, rape seed and sunflowers but barley, other oilseeds, protein and forage crops are significantly more misclassified (*cf.* table 6). This is due to the fact that the transitions of annual crops are less stable and highly vary with regard to agricultural practices and operators in this area.

4.3.2. Impact of parcel size on Site04

Figure 12 shows the impact of parcel size on parcel-wise global accuracies. Since *Site04* is highly fragmented, when keeping only large parcels (area >3 ha), the number of parcels is reduced by 77.5%. Overall accuracies are highly improved by 15%, 5.9% and 8.7% for radar, optical and aggregated optical/radar attributes, respectively). Indeed, due to the limited spatial resolution of Sentinel-1 images, radar attributes are more sensitive to small

Table 6: Confusion matrices using aggregated optical and radar attributes on *Site04*.

	Corn	Barley	O. cereals	Rape Seed	Sun flower	O. oilseeds	Protein	Forage crops	Meadows	Fruit trees	Vignards	Olive groves	Arom crops	Vegetables
	Unstructured Optical radar													
Corn	31	-	-	-	1	2	-	-	-	-	1	-	-	3
Barley	-	47	9-	-	-	-	-	3	37	-	-	-	13	-
O. cereals	-	5	684	-	5	1	-	5	59	-	-	4	25	1
Rape seed	-	-	1	56	-	-	-	-	10	-	-	-	-	-
Sun flower	-	-	1	-	78	-	-	-	2	-	-	-	13	4
O. oilseeds	1	-	-	-	7	18	-	-	4	-	1	-	2	7
Protein	-	2	6	-	-	-	10	1	7	-	-	-	2	-
Forage crops	-	-	18	-	1	-	-	173	239	6	3	9	64	2
Meadows	-	3	16	-	3	1	-	47	1294	-	9	27	77	3
Fruit trees	1	-	1	-	-	-	-	-	52	56	1	9	5	-
Vignards	-	-	-	-	-	-	-	-	18	-	74	4	19	-
Olive groves	-	-	4	-	-	1	-	1	113	1	6	311	26	1
Arom crops	-	-	1	-	-	-	-	-	64	-	2	6	480	2
Vegetables	-	-	2	-	6	4	-	2	18	-	4	6	9	60
	Structured Optical radar													
Corn	28	-	7	-	1	-	-	-	1	-	-	-	1	-
Barley	-	20	123	-	-	-	-	-	47	-	-	-	-	-
O. cereals	1	1	676	-	2	-	-	-	1-2	-	-	-	6	1
Rape seed	-	5	21	35	-	-	-	-	6	-	-	-	-	-
Sun flower	-	-	6	-	67	-	-	1	13	-	-	-	8	3
O. oilseeds	4	-	4	-	7	10	-	-	14	-	-	-	-	1
Protein	-	2	21	-	-	-	-	-	5	-	-	-	-	-
Forage crops	1	-	15	-	3	-	-	25	461	-	-	-	9	1
Meadows	-	1	16	-	1	-	-	2	1456	-	-	1	3	-
Fruit trees	-	-	-	-	-	-	-	-	2	122	1	-	-	-
Vignards	-	-	-	-	-	-	-	-	3	-	112	-	-	-
Olive groves	-	-	1	-	-	-	-	-	3	2	-	458	-	-
Arom crops	-	1	17	-	-	-	-	-	26	-	-	-	511	-
Vegetables	-	-	20	-	10	-	-	-	16	3	-	-	4	58

parcel sizes. When considering parcels greater than 3 ha, radar OA reaches the optical OA at 79.3%.

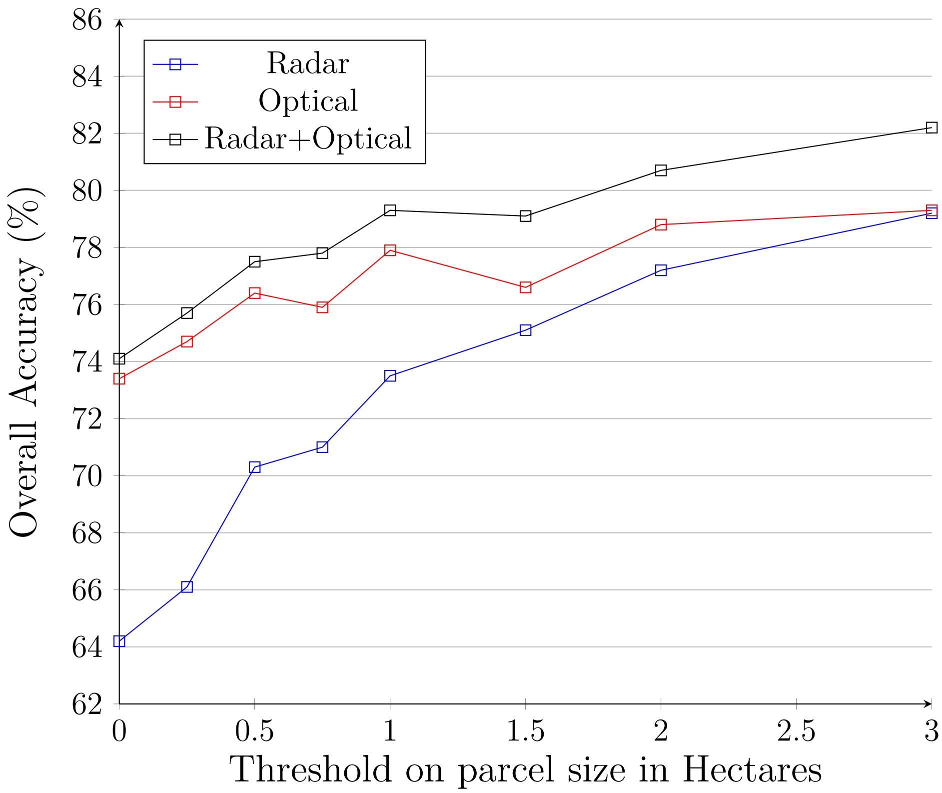

Figure 12: Impact of the parcel size on the global accuracy for parcel-wise classification on *Site04* in the year 2016. x-axis: only parcels whose surface area exceeds the threshold (in ha) are considered.

4.3.3. Quantitative evaluation on Site77

Overall accuracies and F-scores are displayed in Table 7. They are averaged over 10 runs of the random forest classifier. Contrarily to the previous site, on *Site77*, radar attributes give better results than optical attributes (OA = 0.892 Vs. 0.824) for the unstructured approach. This is due to a combination of frequent acquisition problems and high cloud cover in 2016, leading to many missing optical Sentinel-2 data on this study area (cf. Figure 8). In addition, the parcels on *Site77* are larger and thus more compatible with radar Sentinel-1 image spatial resolution. However, aggregated optical and radar attributes still give the best results for the unstructured approach.

Table 7: Global prediction accuracies on *Site77*, using different attribute and methodological configurations.

Config	OA	F-score	Weighted F-score
Unstructured			
Radar	0.892	0.734	0.878
Optical	0.824	0.624	0.809
Radar Optical	0.890	0.744	0.885
Structured			
Radar	0.919	0.776	0.911
Optical	0.870	0.675	0.853
Radar Optical	0.916	0.762	0.906

When looking at per-class accuracies in Table 8, one can see that unlike *Site04*, very good overall accuracies are obtained for annual crops (*Corn* (94.1%), *Barley* (89.8%), *Other cereals* (94.7%), *Rape seed* (95.9%), ...) with the exception of forage crops. Indeed this class is hard to classify using satellite imagery since it is an agronomic class, making it harder to identify using only spectral or radar scattering information even on temporal images. As with *Site04*, Table 8 shows that the *meadows* class is often confused with other classes, particularly *fruit trees* and other cereals. In this case, this is due to the combination of trees and bare soil found in *meadows*, which has a low volumetric radar response.

The structured approach improves overall accuracies by 2.7%, 4.6% and 2.6% for radar, optical, and aggregated optical/radar attributes, respectively. The improvement of temporal structure is lower than for *Site04*, as the initial parcel-wise accuracies are already strong (OA>82%). However, one can observe that the structured approach leads to the best results with radar attributes only.

As for *Site04*, the best improvements occur on permanent crops such as meadows and fruit trees (cf. Table 9). Moreover, the temporal structure improves the prediction of some annual crops such as other cereals, Rape seeds and proteins since they have a high first order transition probability to other cereals.

Table 8: Effect of temporal structure on Classification metrics on *Site77*, using aggregated radar and optical attributes.

Class	**Unstructured**			**Structured**		
Class	F-score	Recall	Precision	F-score	Recall	Precision
Corn	0.941	0.929	0.953	0.878	0.831	0.935
Barley	0.898	0.937	0.862	0.816	0.785	0.849
Other cereals	0.947	0.956	0.9378	0.954	0.941	0.968
Rape seed	0.959	0.975	0.944	0.969	0.985	0.954
Protein	0.949	0.932	0.968	0.953	0.967	0.939
Fiber plants	0.974	1	0.950	0	0.1	0
Forage crops	0	0.1	0	0.705	0.778	0.648
Meadows	0.868	0.814	0.930	0.955	0.943	0.967
Fruit trees	0.010	0.090	0	0.940	1	0.892
Vegetables	0.895	0.914	0.877	0.451	0.970	0.297

4.3.4. Impact of parcel size on Site77

Figure 13 shows the impact of parcel size on the global accuracies of the parcel-wise prediction. Since *Site77* is less fragmented than *Site04*, keeping only large parcels (area $>$ 3 ha), reduces the number of parcels by % 52,3%.

As with *Site04*, when considering larger parcels, the overall accuracy is greatly improved with radar attributes (by 7.3% reaching 97.1%), which confirms the high sensitivity of radar images to parcel size.

For optical attributes, the relation between parcel size and accuracy is less clear. This may be due to the data imbalance, with some classes that are more present in small parcels (0.5-1.5 ha) and which are well identified such as Rape seed or Protein. Thus, removing these small parcels may decrease the overall accuracy. The classes that are responsible for the higher OA observed between 0 and 0.75 ha are *Fiber plants* and *Meadows* where *meadows* parcels are much smaller than for other classes and that *fiber plants* parcels are homogeneous in terms of area (*cf.* Figure 5).

As for radar data sensitivity to limited parcel sizes, some improvements of our framework could be undertaken on radar pre-processing. Indeed, the GRD Sentinel-1 images were used as input images when each GRD radar pixel is already an average of 5 pixels of the SLC (Single Look Complex). Using SLC images directly would allow us to achieve greater spatial resolution. Then, a

Table 9: Confusion matrices using aggregated optical and radar attributes on *Site77*.

	Corn	Barley	Other cereals	Rape Seed	Fiber plants	Protein	Forage crops	Meadows	Fruit trees	Vegetables
	Unstructured Optical radar									
Corn	119	-	-	-	-	-	-	6	-	-
Barley	1	48	2	-	1	-	-	3	-	-
Other cereals	-	2	309	-	-	-	-	19	-	1
Rape seed	-	-	-	38	-	-	-	3	-	-
Fiber plants	-	-	-	-	27	-	-	1	-	-
Protein	-	-	-	-	1	9	-	-	-	-
Forage crops	-	-	1	-	-	-	-	20	-	-
Meadows	10	1	9	1	-	-	-	276	-	1
Fruit trees	-	-	-	-	-	-	-	12	-	-
Vegetables	1	-	1	-	-	-	-	1	-	27
	Structured Optical radar									
Corn	118	1	1	-	-	-	3	2	-	-
Barley	1	48	5	-	-	-	-	1	-	-
Other cereals	-	2	321	1	-	-	-	7	-	-
Rape seed	-	-	1	39	-	-	-	1	-	-
Fiber plants	-	-	1	-	27	-	-	-	-	-
Protein	1	8	-	-	1	-	-	-	-	-
Forage crops	-	1	2	-	-	-	13	5	-	-
Meadows	4	-	4	-	-	-	1	289	-	-
Fruit trees	-	-	-	-	-	-	-	-	12	-
Vegetables	19	-	2	-	-	-	-	-	-	9

simple speckle filter was used [30] on a restricted local neighborhood (5×5). This is not a problem for large parcels as the radar scattering coefficients are averaged afterwards at the agricultural parcel level. However, when parcel surface areas approach the Sentinel-1 spatial resolution, this method is no longer suitable. The robustness of adaptive radar speckle filtering to small objects should be investigated [35]. Finally, using a very high spatial resolution Digital Terrain Model instead of the SRTM could improve absolute

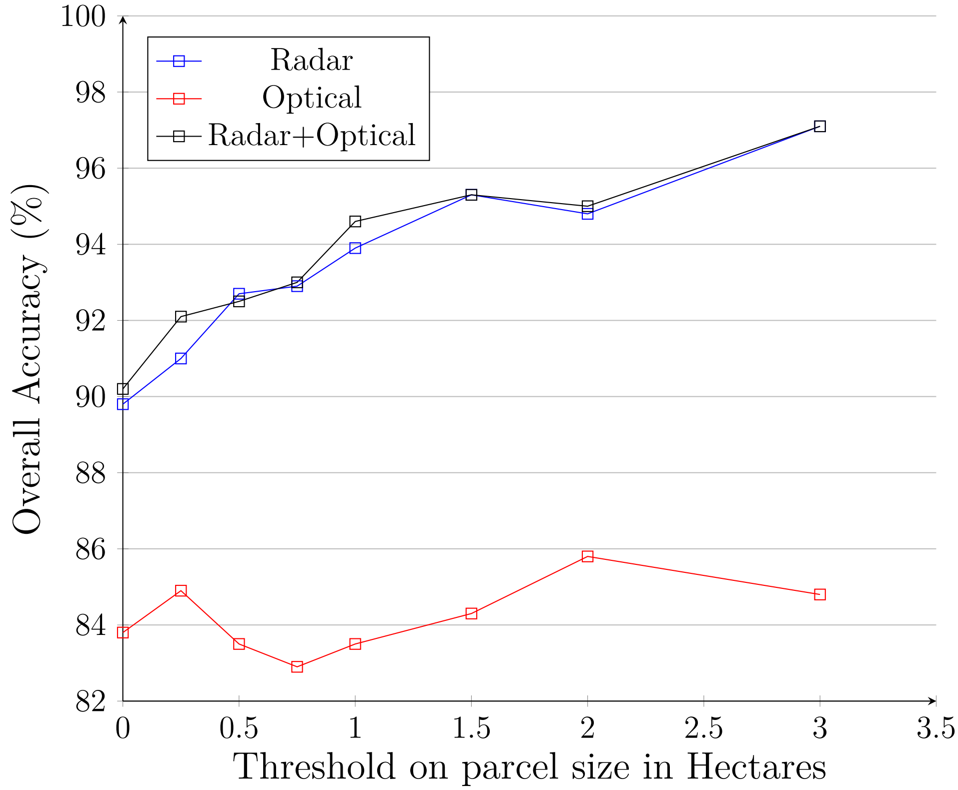

Figure 13: Unstructured parcel-based classification for year 2016, *Site77* - Impact of parcel size on accuracy; x-axis: only parcels whose surface area exceeds the threshold (in ha) are considered.

orthorectification accuracy of Sentinel-1 images and allows us to correct radar scattering coefficient from the effect of terrain slope (γ_0 calibration). As a result, the intra-class variability of signal could be reduced.

5. Conclusion and perspectives

This study demonstrated the efficiency of an automatic prediction of crop types using Sentinel 1 and 2 images and LPIS archives as a first step for an automatic filled pre-declaration intended for farmers.

From a thematic point of view, this paper demonstrates the efficiency of multi-temporal and multi-source Sentinel (optical and radar) images for crop type classification on two different sites. Very satisfactory discrimination results are obtained even with a large number of classes (>10). The remaining limitations are essentially the parcel size with regard to the spatial resolution of images and the complexity of the nomenclature. Results highlight the high sensitivity of radar data to small parcel sizes, especially on *Site04*. This issue can be reduced by a refining the preprocessing framework of radar data. Moreover, the complexity of certain agronomic classes such as forage crops should be discussed with agronomists in order to design a proper hierarchical classification.

From a methodological point of view, we integrated the temporal structure by automatically modeling the crop rotations using prevision editions of LPIS. This model appears to be very efficient, improving the global classification prediction of crop types. However, the impact of integrating temporal structure varies highly among classes. Although a positive impact is demonstrated on permanent crops using first order crop transitions, this impact is fairly limited or even detrimental for annual crops. Other transition orders should be investigated to confirm the interest of temporal structure for annual crops. Finally, thanks to the large volume of available LPIS data that can be used as ground truth, and the free availability of numerous Sentinel images, deep learning methods should be tested to learn parcels' embeddings.

Acknowledgments

The authors want to thank the ASP (French payment agency) and the French agricultural ministry for the rich discussions and their guidance for the nomenclature choice and crop rotation schemes.

References

[1] European Commission, Towards future Copernicus service components in support to agriculture?, https://ec.europa.eu/jrc/sites/jrcsh/files/Copernicus_concept_note_agriculture.pdf, 2016.

[2] Y. Palchowdhuri, R. Valcarce-Diñeiro, P. King, M. Sanabria-Soto, Classification of multi-temporal spectral indices for crop type mapping: a case study in coalville, uk, The Journal of Agricultural Science 156 (2018) 24–36.

[3] J. Inglada, M. Arias, B. Tardy, O. Hagolle, S. Valero, D. Morin, G. Dedieu, G. Sepulcre, S. Bontemps, P. Defourny, et al., Assessment of an operational system for crop type map production using high temporal and

spatial resolution satellite optical imagery, Remote Sensing 7 (2015) 12356–12379.

[4] L. Breiman, Random forests, Machine learning 45 (2001) 5–32.

[5] M. Immitzer, F. Vuolo, C. Atzberger, First experience with Sentinel-2 data for crop and tree species classifications in central Europe, Remote Sensing 8 (2016) 166.

[6] N. Kussul, G. Lemoine, F. J. Gallego, S. V. Skakun, M. Lavreniuk, A. Y. Shelestov, Parcel-based crop classification in Ukraine using Landsat-8 data and Sentinel-1a data, IEEE Journal of Selected Topics in Applied Earth Observations and Remote Sensing 9 (2016) 2500–2508.

[7] Sen2-Agri, Czech agriculture national demonstrator - final report. http://www.esa-sen2agri.org/wp-content/uploads/docs/CzechAgri%20Final%20Report%201.2.pdf, 2018. Accessed on February 6, 2018.

[8] Z. Berzsenyi, B. Győrffy, D. Lap, Effect of crop rotation and fertilisation on maize and wheat yields and yield stability in a long-term experiment, European Journal of Agronomy 13 (2000) 225–244.

[9] D. L. Karlen, E. G. Hurley, S. S. Andrews, C. A. Cambardella, D. W. Meek, M. D. Duffy, A. P. Mallarino, Crop rotation effects on soil quality at three northern corn/soybean belt locations, Agronomy journal 98 (2006) 484–495.

[10] D. Karlen, G. Varvel, D. G. Bullock, R. Cruse, Crop rotations for the 21st century, Advances in agronomy 53 (1994).

[11] S. Dogliotti, W. Rossing, M. Van Ittersum, ROTAT, a tool for systematically generating crop rotations, European Journal of Agronomy 19 (2003) 239–250.

[12] M. Castellazzi, G. Wood, P. J. Burgess, J. Morris, K. Conrad, J. Perry, A systematic representation of crop rotations, Agricultural Systems 97 (2008) 26–33.

[13] J. Dury, N. Schaller, F. Garcia, A. Reynaud, J. E. Bergez, Models to support cropping plan and crop rotation decisions. a review, Agronomy for sustainable development 32 (2012) 567–580.

[14] J. Aurbacher, S. Dabbert, Generating crop sequences in land-use models using maximum entropy and Markov chains, Agricultural Systems 104 (2011) 470–479.

[15] N. K. Detlefsen, A. L. Jensen, Modelling optimal crop sequences using network flows, Agricultural Systems 94 (2007) 566–572.

[16] J. E. Olesen, M. Trnka, K. Kersebaum, A. Skjelvåg, B. Seguin, P. Peltonen-Sainio, F. Rossi, J. Kozyra, F. Micale, Impacts and adaptation of European crop production systems to climate change, European Journal of Agronomy 34 (2011) 96–112.

[17] J. Aurbacher, P. S. Parker, G. A. C. Sánchez, J. Steinbach, E. Reinmuth, J. Ingwersen, S. Dabbert, Influence of climate change on short term management of field crops–a modelling approach, Agricultural Systems 119 (2013) 44–57.

[18] F. Le Ber, M. Benoît, C. Schott, J.-F. Mari, C. Mignolet, Studying crop sequences with CarrotAge, a HMM-based data mining software, Ecological modelling 191 (2006) 170–185.

[19] M. Schönhart, E. Schmid, U. A. Schneider, CropRota–a crop rotation model to support integrated land use assessments, European Journal of Agronomy 34 (2011) 263–277.

[20] J. Bachinger, P. Zander, ROTOR, a tool for generating and evaluating crop rotations for organic farming systems, European Journal of Agronomy 26 (2007) 130–143.

[21] Y. Xiao, C. Mignolet, J.-F. Mari, M. Benoít, Modeling the spatial distribution of crop sequences at a large regional scale using land-cover survey data: A case from France, Computers and Electronics in Agriculture 102 (2014) 51–63.

[22] C. Boryan, Z. Yang, R. Mueller, M. Craig, Monitoring us agriculture: the us department of agriculture, national agricultural statistics service, cropland data layer program, Geocarto International 26 (2011) 341–358.

[23] B. Leteinturier, J. Herman, F. De Longueville, L. Quintin, R. Oger, Adaptation of a crop sequence indicator based on a land parcel management system, Agriculture, Ecosystems & Environment 112 (2006) 324–334.

[24] J. Osman, J. Inglada, J.-F. Dejoux, Assessment of a Markov logic model of crop rotations for early crop mapping, Computers and Electronics in Agriculture 113 (2015) 234–243.

[25] L. Aurdal, R. B. Huseby, L. Eikvil, R. Solberg, D. Vikhamar, A. Solberg, Use of hidden Markov models and phenology for multitemporal satellite image classification: Applications to mountain vegetation classification, in: Proc. Int. Workshop Analysis Multi-Temporal Remote Sensing Images, pp. 16–18.

[26] P. B. C. Leite, R. Q. Feitosa, A. R. Formaggio, G. A. da Costa, O. Pedro, K. Pakzad, I. D. Sanches, Hidden Markov Models for crop recognition in remote sensing image sequences, Pattern Recognition Letters 32 (2011) 19–26.

[27] S. Siachalou, G. Mallinis, M. Tsakiri-Strati, A hidden Markov models approach for crop classification: Linking crop phenology to time series of multi-sensor remote sensing data, Remote Sensing 7 (2015) 3633–3650.

[28] C. Conrad, S. Dech, O. Dubovyk, S. Fritsch, D. Klein, F. Löw, G. Schorcht, J. Zeidler, Derivation of temporal windows for accurate crop discrimination in heterogeneous croplands of Uzbekistan using multitemporal RapidEye images, Computers and Electronics in Agriculture 103 (2014) 63–74.

[29] B. Kenduiywoa, D. Bargiel, U. Soergel, Spatial-temporal Conditional Random Fields crop classification from Terrasar-X images, ISPRS Annals of the Photogrammetry, Remote Sensing and Spatial Information Sciences 2 (2015) 79.

[30] J.-S. Lee, Digital image enhancement and noise filtering by use of local statistics, IEEE Transactions on Pattern Analysis and Machine Intelligence (1980) 165–168.

[31] A. Veloso, S. Mermoz, A. Bouvet, T. Le Toan, M. Planells, J.-F. Dejoux, E. Ceschia, Understanding the temporal behavior of crops using Sentinel-1 and Sentinel-2-like data for agricultural applications, Remote Sensing of Environment 199 (2017) 415–426.

[32] J. Inglada, OTB Gapfilling, a temporal gapfilling for image time series library, Zenodo, 2016. Http://doi.org/10.5281/zenodo.45572.

[33] D. Liu, K. Song, J. R. Townshend, P. Gong, Using local transition probability models in Markov random fields for forest change detection, Remote Sensing of Environment 112 (2008) 2222 – 2231.

[34] C. D. Manning, P. Raghavan, H. Schütze, et al., Introduction to information retrieval, volume 1, Cambridge university press Cambridge, 2008.

[35] C.-A. Deledalle, L. Denis, F. Tupin, A. Reigber, M. Jäger, NL-SAR: A unified nonlocal framework for resolution-preserving (pol)(in) SAR denoising, IEEE Transactions on Geoscience and Remote Sensing 53 (2015) 2021–2038.